PAPER

Intense pulsed light, a promising technique to develop molybdenum sulfide catalysts for hydrogen evolution

IOP Publishing Nanotechnology
Nanotechnology 30 (2019) 175401 (8pp) https://doi.org/10.1088/1361-6528/aaffac

Intense pulsed light, a promising technique to develop molybdenum sulfide catalysts for hydrogen evolution

Alexander Gupta[2], Krishnamraju Ankireddy[2], Bijendra Kumar[2], Adel Alruqi[3], Jacek Jasinski[2], Gautam Gupta[1] and Thad Druffel[1]

[1] University of Louisville, Department of Chemical Engineering, Louisville, KY 40292, United States of America
[2] University of Louisville, Conn Center for Renewable Energy Research, Louisville, KY 40292, United States of America
[3] University of Louisville, Department of Physics and Astronomy, Louisville, KY 40292, United States of America

E-mail: thad.druffel@louisville.edu

Received 23 November 2018, revised 20 December 2018
Accepted for publication 17 January 2019
Published 18 February 2019

Abstract

We have demonstrated a simple and scalable fabrication process for defect-rich MoS_2 directly from ammonium tetrathiomolybdate precursor using intense pulse light treatment in milliseconds durations. The formation of MoS_2 from the precursor film after intense pulsed light exposure was confirmed with XPS, XRD, electron microscopy and Raman spectroscopy. The resulting material exhibited high activity for the hydrogen evolution reaction (HER) in acidic media, requiring merely 200 mV overpotential to reach a current density of 10 mA cm^{-2}. Additionally, the catalyst remained highly active for HER over extended durability testing with the overpotential increasing by 28 mV following 1000 cycles. The roll-to-roll amenable fabrication of this highly-active material could be adapted for mass production of electrodes comprised of earth-abundant materials for water splitting applications.

Supplementary material for this article is available online

Keywords: MoS_2, intense pulsed light, hydrogen evolution

(Some figures may appear in colour only in the online journal)

1. Introduction

Hydrogen production via electrocatalysis is a promising route for storing excess energy from renewable sources (such as wind or solar) during off-peak energy consumption hours. In addition to its use as an energy carrier, molecular hydrogen is an important chemical feedstock with applications in ammonia production, hydrocracking, hydrodesulfurization, and other industries. Platinum and other noble metals are efficient catalysts for the hydrogen evolution reaction (HER) [1]; however, they are scarce and expensive [2]. Earth-abundant alternative catalysts [3], including metal carbides, nitrides, and sulfides [4, 5], are promising candidates to achieve electrocatalytic hydrogen production [6].

Among these catalysts, molybdenum disulfide (MoS_2) has been explored widely for hydrogen production [7, 8] due to its environmental benignity, high stability in acidic environments, and good catalytic activity. MoS_2 is a transition metal dichalcogenide with an Mo layer sandwiched between two sulfur layers with weak Van der Waals forces in a trigonal prismatic arrangement [9, 10]. The edges of sheet-like MoS_2 are active sites for HER, with the basal plane being catalytically inert, so a greater concentration of edge sites is associated with better catalytic activity [11]. There has been tremendous effort put into the preparation of active MoS_2 structures via solvent-assisted exfoliation [12], chemical exfoliation [13, 14], hydrothermal synthesis [15], intercalation-aided exfoliation [16], chemical vapor deposition [17, 18], thermal annealing of

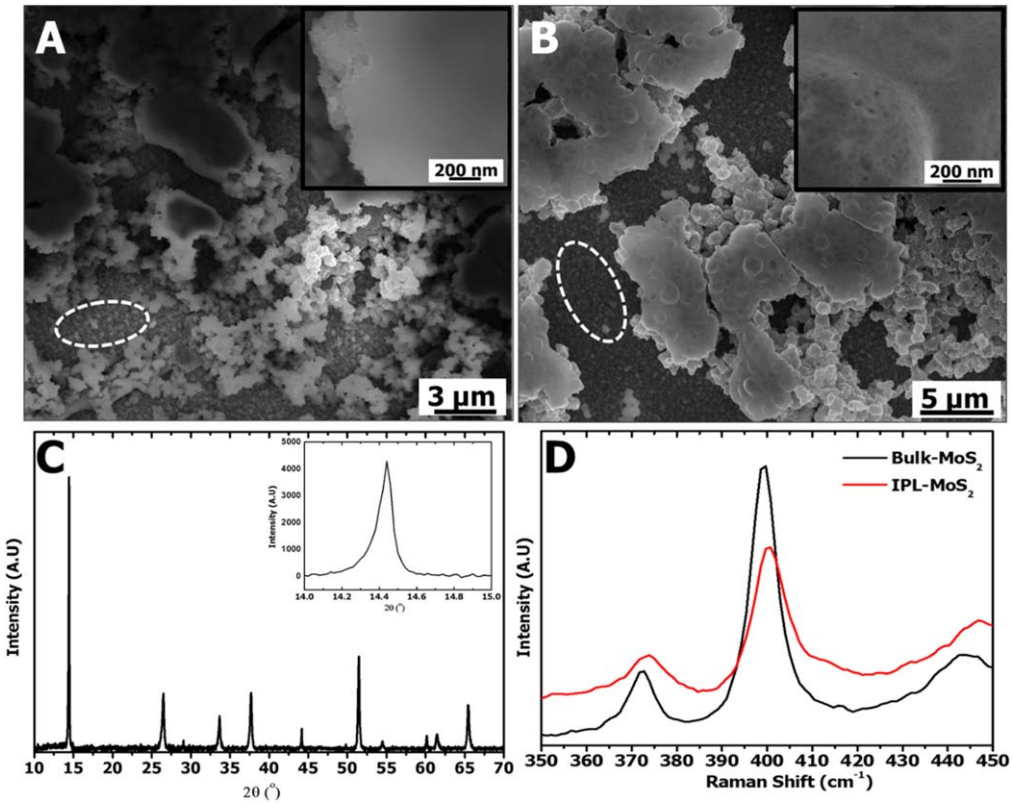

Figure 1. MoS_2 structural analysis (A) ammonium thiomolybdate precursor film on FTO-coated glass substrate (B) IPL treated MoS_2 film on FTO-coated glass substrates (white dotted circles display the FTO surface morphology) (C) XRD spectrum of IPL-MoS_2 film, (D) Raman spectra from bulk MoS_2 and IPL-MoS_2 structures.

MoS_2 precursor materials [19], and electrochemical synthesis [20]. The large-scale preparation of MoS_2 films by chemical vapor deposition, and nanosheets by solution-based chemical exfoliation, has also been reported [21]. Industrial implementation of most of these fabrication methods is somewhat impractical due to sophisticated synthesis procedures with processing steps including high vacuum, high temperature, H_2S gas flow, and/or inert atmosphere conditions. Here, we report a novel one-step, extremely fast, and scalable fabrication method for defect-rich MoS_2 using the intense pulsed light (IPL) technique.

IPL, also known as photonic sintering, imparts rapid intense pulses of light to provide localized heating and/or induce chemical reactions in an absorbing thin film. The IPL unit essentially contains a xenon flash lamp, a capacitor bank, and coil circuitry which cooperatively generate a burst of intense light. The treatment is carried out within a millisecond time frame which is desirable from a processing standpoint. The light energy is absorbed by the thin film and almost immediately released as heat, inducing very localized temperatures of several hundred degrees centigrade. Process parameters include the input energy density, pulse duration, and number of pulses. The IPL technique has been utilized for processing metal nanoparticles and semiconductor materials for various applications [22].

This study highlights the rapid means of preparing MoS_2 structures with high edge site concentration from precursor-coated films using IPL for the first time. The structural properties of the resulting material (IPL-MoS_2) were analyzed using x-ray diffraction (XRD), Raman, scanning electron microscopy, transmission electron microscopy (TEM) and x-ray photoelectron spectroscopy (XPS) and compared with those of bulk MoS_2. IPL-MoS_2 was further characterized in terms of its electrochemical activity for HER and compared with bulk MoS_2. Electrochemical characterization reveals that IPL-MoS_2 exhibits catalytic activity superior to bulk crystalline MoS_2 and is among the most highly active reported MoS_2 catalysts obtained from various treatments for HER [6].

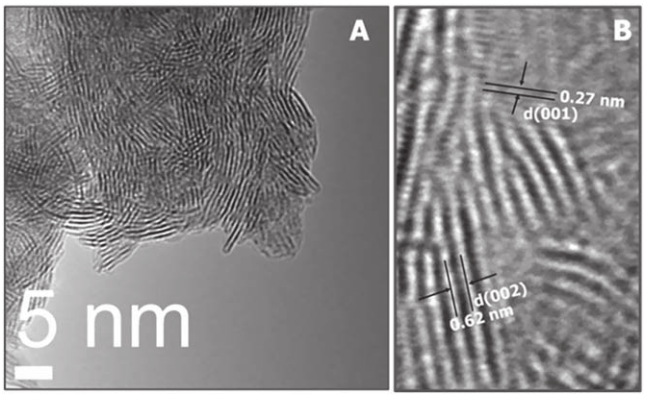

Figure 2. High-resolution TEM images of IPL-MoS_2 nanosheets (A) Defect-rich MoS_2 nanosheets (B) TEM image showing the interplanar spacing between (100) planes and layer-to-layer spacing.

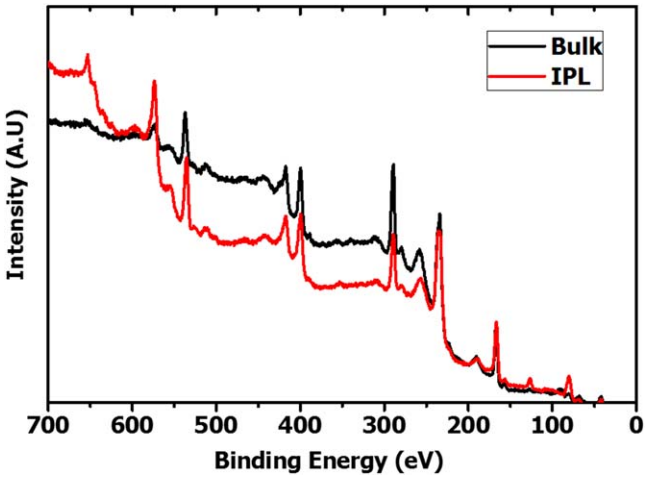

Figure 3. XPS spectrum of bulk MoS_2 and IPL-MoS_2 samples.

2. Methods

2.1. Materials

Bulk molybdenum sulfide powder with an average particle size of 6 μm was purchased from Sigma Aldrich. Ammonium tetrathiomolybdate powder was supplied by Beantown Chemical. Ethanol (200 proof) was obtained from Decon Labs. Twice-deionized Millipore water (18 MΩ cm) was used. FTO-coated glass was obtained from Hartford Glass Company, Hartford City, IN. Sulfuric acid (ACS grade) was purchased from VWR. Compressed nitrogen and hydrogen gases were provided by Welders Supply, Louisville, KY.

2.2. MoS_2 film preparation and IPL processing

The precursor solution was prepared by mixing 0.157 g of ammonium tetrathiomolybdate in 2:1 v/v water and ethanol solvent for a total of 6 ml. The solution was sonicated for two hours and subsequently filtered through a 250 nm nylon filter. The same procedure was used to prepare the bulk crystalline MoS_2 solution. The filtered solution was drop casted on FTO-coated glass substrates (for material characterization) or glassy carbon electrodes (GCE, for electrochemical testing) with a loading of approximately 1.3 mg cm^{-2}. The GCEs were rotated (∼400 RPM) during dropcasting to obtain a relatively uniform film, while the FTO substrates were not. The air-dried films were IPL treated with a total number of 10 repeated pulses with each pulse producing 25 J cm^{-2} energy density and having a 2 ms duration. The Sinteron 2000-L IPL apparatus and full-spectrum UV-to-near-IR lamp were purchased from xenon.

2.3. Experimental set-up for HER

Electrochemical characterization was carried out using a Metrohm Autolab PGSTAT302N potentiostat/galvanostat in potentiostat mode with a MSR electrode rotator from Pine Research. Replaceable-tip glassy carbon working electrodes were purchased from Pine Research (E4TQ Changedisk series). A five-neck electrochemical cell from Pine Research was filled with 0.5 M H_2SO_4 electrolyte. A graphite rod inside a glass frit (Pine Research) was used as the counter electrode. An Ag/AgCl reference electrode, calibrated versus RHE (223.1 mV versus RHE), was used to determine the absolute potential throughout electrochemical experiments. A glass diffuser (Pine Research) was used to bubble gas into the electrolyte. Platinum meshes (Alfa Aesar, 99.9% metals basis) were used to calibrate measured potentials versus RHE. A platinum ring (Pine Research, E6R2 Fixed-Disk RRDE Tip) was used to measure the HER activity of platinum.

2.4. Characterization of MoS_2 films

XRD was carried out using a Bruker Discovery D8 x-ray diffractometer equipped with an x-ray source of Cu Kα ($\lambda = 0.1548$ nm) and operated at a scan rate of 2 s/step and a step size of 0.02°. Raman spectroscopy was performed using a Renishaw Raman Spectrometer equipped with a red laser of 632 nm. The power of the red laser was kept below 1 mW to prevent over heating of the sample, and the emission was collected with an integrated CCD camera by dispersing with a 1800 lines mm^{-1} grating. TEM analysis was carried out using a FEI Tecnai F20 TEM equipped with a field emission gun (FEG) and operated at 200 kV of accelerating voltage. Microstructures of the films were characterized using a FEI Nova NanoSEM 600 with an accelerating voltage of 10 kV and a working distance of 5 mm. XPS was carried out using a VG Scientific MultiLab 3000 ultra-high vacuum surface analysis system with CLAM4 hemispherical electron energy analyzer and a dual-anode Mg/Al x-ray source. All measurements were performed using non-monochromatic Al K_α ($h\nu = 1486.6$ eV) x-ray radiation under a base chamber pressure in the low 10^{-8} Torr range. For each sample, a survey scan from 0 to 1000 eV was collected to identify all elemental peaks. This was followed by the acquisition of high-resolution Mo 3d, S 2p, C 1s and O 1s spectra. An intrinsic C 1s peak at 284.5 eV was used for the binding energy calibration. The analysis of XPS spectra (background subtraction and peak deconvolution) was performed using XPSPEAK4.1 software. The background curves were fitted with a Shirley function.

Electrochemical characterization was done using linear sweep voltammetry, cyclic voltammetry, and frequency response analysis techniques. To obtain polarization/Tafel plots, the potential was swept from 0.1 to −0.6 V versus RHE at a rate of 5 mV s^{-1}. For activation/durability testing, the potential was swept from 0.1 to −0.35 and back to 0.1 V versus RHE at 50 mV s^{-1} repeatedly. All measured potentials were calibrated to the RHE scale after the experiment (to avoid platinum contamination) by saturating the electrolyte with H_2 gas, conducting cyclic voltammetry repeatedly between platinum working and counter electrodes, and taking the average potential versus the reference electrode at zero current.

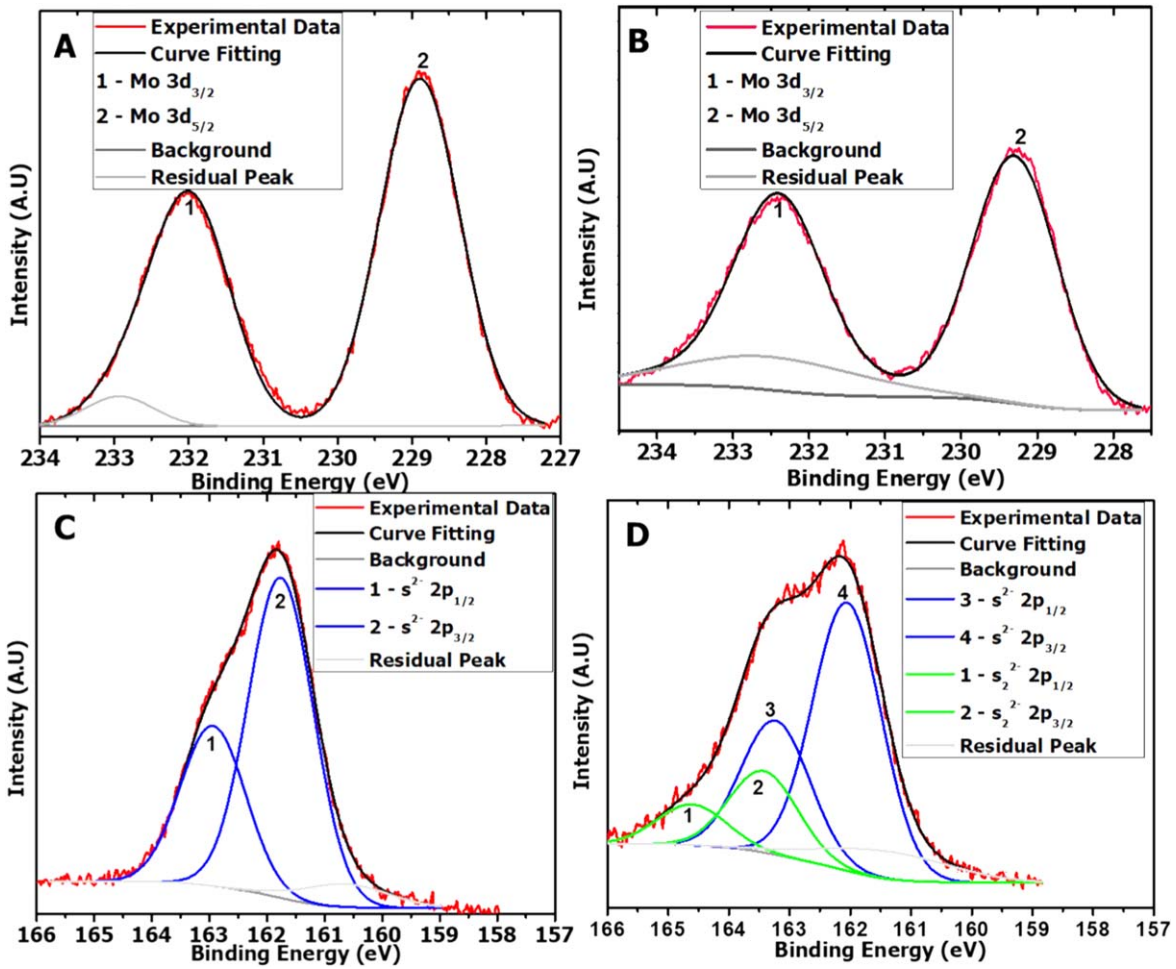

Figure 4. XPS elemental analysis of bulk MoS_2 (A) and (C) and IPL-MoS_2 (B) and (D) structures.

3. Results and discussion

The surface morphology analysis of the ammonium tetrathiomolybdate precursor film before and after IPL exposure reveals an obvious morphological change after IPL treatment (figures 1(A) and (B)). The films consist of thick micron-scale assemblies. However, the larger features with smooth surface morphology transformed to aggregates after IPL, which is similar to sintering that has been demonstrated before with IPL [23–25]. The high-resolution images of IPL-treated film clearly exhibit rough surface morphology compared to as-deposited precursor film. To investigate whether this morphological change led to MoS_2 structure, XRD was carried out on IPL-MoS_2. The crystallographic structural analysis of IPL-MoS_2 revealed the successful conversion of precursor material into MoS_2 structure. The XRD reflection peak at 14.4°, corresponds to hexagonal MoS_2 phase (JCPDS card No. 73-1508) (figure 1(C)). The majority of the other reflections (26.5°, 33.5°, 37.7°, 51.6°, 54.4°, 61.6° and 65.5°) originate from the underlying FTO substrate. Comparative XRD patterns (figure S1 is available online at stacks.iop.org/NANO/30/175401/mmedia) show the presence of the reflection at 14.4° in IPL-MoS_2 and the absence of this reflection in the precursor. The calculated d-spacing, using the diffraction angle at 14.4° which corresponds to the (002) crystal plane, is 0.615 nm which is similar to that of 2H–MoS_2 (0.62 nm).

Further investigation of structural transformation from precursor to MoS_2 nanosheets was carried out using Raman spectroscopy and compared with the spectra from bulk MoS_2 structures. The Raman spectra reveal that E2g (373.8 cm^{-1}) and A1g (400.2 cm^{-1}) peaks from IPL-MoS_2 match the corresponding E2g (372.3 cm^{-1}) and A1g (399.2 cm^{-1}) peaks from bulk MoS_2, confirming the IPL-assisted conversion of precursor film to MoS_2 (figure 1(D)). Raman spectra from 300 to 500 cm^{-1} are shown in figure S2. The dominant phase exhibited by both IPL and bulk MoS_2 materials was 2H–MoS_2. There is a broad peak between 440 and 450 cm^{-1}, and attributing this peak to MoS_2 is an open question. The peak at 454 cm^{-1} was previously assigned to the double frequency of the LA(M) mode (227 cm^{-1}), and the peak at 440 cm^{-1} was predicted to be Mo–S vibrations for oxysulfide species [26–28]. However, further investigation is required to confirm if there is any oxysulfide species in IPL and bulk MoS_2 materials which is beyond the scope of this study.

Further probing of morphological and structural properties of the IPL-MoS_2 was conducted using TEM. Analysis of the films reveals that there are highly-corrugated lattice

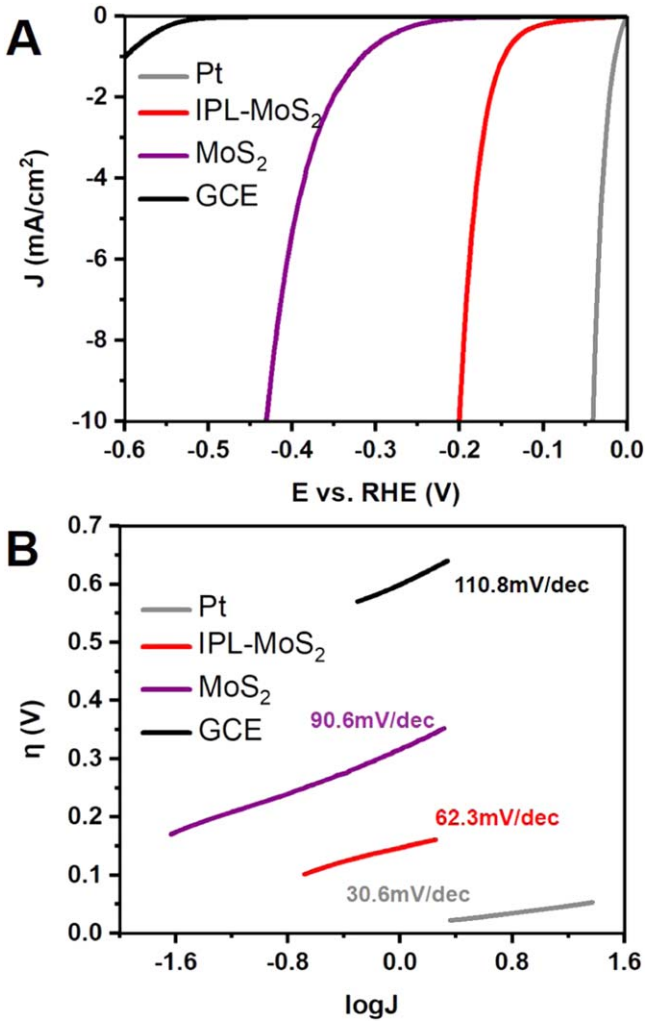

Figure 5. Electrochemical activity of the molybdenum sulfide catalyst following IPL treatment (IPL-MoS_2, red trace) in 0.5 M H_2SO_4. Included for comparison purposes are electrochemical activities of platinum metal (Pt, gray trace), bulk crystalline molybdenum sulfide (MoS_2, purple trace), and bare glassy carbon electrode (GCE, black trace) in 0.5 M H_2SO_4. The polarization plot (A) shows that the molybdenum sulfide catalyst exhibits high activity for HER, and the Tafel plot (B) compares kinetic attributes of various materials for HER.

fringes across the sample. This implies that there are many defects and distortions within the structures. TEM images reveal mostly short clusters with discontinuous, bending, disjointed, and curved basal planes resulting in a highly defective MoS_2 structure (figure 2(A)). The interlayer d-spacing is found to be 0.62 nm (figure 2(B)), confirming the XRD results. The individual planes are curved or bent which indicates disordered atomic arrangement. This, together with the fact that most clusters are short segments, indicates high density of edge sites, which are responsible for improved HER performance. High-resolution TEM images were obtained at different areas of the sample (figure S3); these micrographs exhibited very similar defect structure which signifies homogeneity of the sample. To investigate the mechanism of IPL-assisted MoS_2 formation from the precursor materials, XPS analysis of molybdenum (Mo) and sulfur (S) elements in both bulk MoS_2 and IPL-MoS_2 was carried out.

A survey scan was acquired from 1 to 1000 eV. Detailed analysis on Mo and S elements was subsequently conducted by collecting high-resolution spectra of main Mo and S peaks. The survey spectra from IPL-MoS_2 and bulk MoS_2 are similar to each other (figure 3).

Mo and S peaks were detected in addition to C and O impurity peaks. The binding energies of Mo $3d_{5/2}$ are 228.9 and 229.3 eV for bulk MoS_2 and IPL-MoS_2 respectively, indicating +4 oxidation state for the Mo ion [29], whereas the binding energies for the Mo $3d_{3/2}$ are 232 and 232.4 eV for the bulk and IPL-MoS_2 samples respectively (figures 4(A) and (B)). The binding energy difference between Mo $3d_{5/2}$ and Mo $3d_{3/2}$ is 3.1 eV for the both bulk and IPL-MoS_2 samples. The energy difference of 3.1 eV is a characteristic of Mo species. The S 2p spectrum of IPL-MoS_2 exhibited a broad peak which was further deconvoluted. This resulted in two doublets with the S $2p_{3/2}$ and S $2p_{1/2}$ states. The highest area doublet exhibited peaks at 162.0 and 163.3 eV for S $2p_{3/2}$ and S $2p_{1/2}$ states respectively, whereas the lowest area doublet displayed peaks at 163.5 and 164.6 eV for S $2p_{3/2}$ and S $2p_{1/2}$ states respectively. In case of bulk MoS_2, the S $2p_{3/2}$ and S $2p_{1/2}$ states showed peaks at 161.8 and 163 eV, respectively. The single doublet with S $2p_{3/2}$ around 161.8 eV is typical for S^{2-} ligands that form MoS_2. This suggests that the bulk MoS_2 powder might not have any other forms of S ligands, whereas the second doublet peak from IPL-MoS_2 with S $2p_{3/2}$ at 163.5 eV indicates the existence of S_2^{2-} ligands.

Muijsers *et al* conducted a sulfidation study on molybdenum oxide. The peak positions of S 2p for different intermediate compounds and the final MoS_2 structure after thermal decomposition has been assigned [29, 30]. In the case of the IPL-MoS_2 sample, the S $2p_{3/2}$ peak at 163.5 eV can be attributed to bridging/apical S^{2-}. This indicates the existence of a small portion of intermediate complexes present in the IPL-MoS_2 sample. The area ratio of the lowest intensity doublet to the highest intensity doublet is 0.3, which signifies that most of the precursor transformed to MoS_2 with minor amounts of intermediate complexes. The melting temperature of ammonium tetrathiomolybdate is approximately 155 °C, which is much lower than the temperature attained from the IPL process. This rapid thermal process might cause decomposition and sublimation of the sulfur and ammonium, which might create a large defect density in the film.

In addition, rapid heat treatment of the samples in milliseconds time scale might not fully reduce some of the sulfur atoms which can form bridging or terminal groups of MoS_2 structure. The IPL treated films still might have different forms of S atoms along with the S^{2-} basal plane.

Based on the preceding observations, and other observations reported in literature, we propose the following mechanism for the conversion of tetrathiomolybdate to molybdenum disulfide [31]:

$$MoS_4^{2-} + 2NH_4^+ \xrightarrow{\Delta} MoS_2 + H_2S + S + 2NH_3.$$

Table 1. Comparison of HER overpotentials and Tafel slopes for IPL-MoS_2 and other reported molybdenum sulfide catalysts.

MoS_2 catalyst	Overpotential (mV) @ 10 mA cm^{-2}	Tafel slope (mV dec^{-1})
IPL-MoS_2 (this study)	200	62.3
Core–shell MoO_3–MoS_2 nanowires [34]	~250	50–60
MoS_2 NSs-550 [35]	~200	68
Amorphous molybdenum sulfide [36]	200	60
1T-MoS_2 [13]	187	43
Defect-rich MoS_2 nanosheets [37]	~150	50
MoS_2/RGO [38]	~150	41

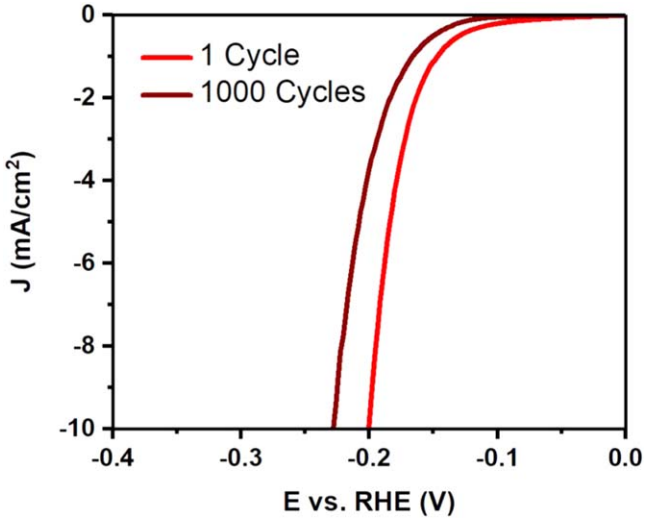

Figure 6. Polarization curves for IPL-MoS_2 after activation (1 Cycle, red trace) and after 1000 cycles at reductive potential (1000 cycles, brown trace).

Electrochemical characterization was carried out on GCEs in a three-electrode cell. Dropcasting the precursor solution onto the GCE over rotation and then treating with IPL yields a rough IPL-MoS_2 film with thickness of approximately 20 μm (figure S4). The diffusion length of a light pulse through a metal or semiconductor film has been shown to be on the order of hundreds of micrometers [32]. Therefore, local variations of film thickness should not significantly affect the conversion. Other factors affecting the conversion include number of pulses, energy density, and pulse duration [33]. Detailed mechanistic and optimization studies on the IPL-assisted conversion of ammonium tetrathiomolybdate to IPL-MoS_2 are currently underway. All potentials have been iR compensated and calibrated versus RHE. A polarization plot comparing the activity of IPL-MoS_2 with other representative HER catalysts is depicted in figure 5(A). IPL-MoS_2 exhibits an onset overpotential for HER around 100 mV with an overpotential required to reach 10 mA cm^{-2} (a benchmark for solar water-splitting applications) of approximately 200 mV. IPL-MoS_2 shows similar activity on FTO-coated glass substrate (figure S5). The low overpotential observed for IPL-MoS_2 is compared with overpotentials reported for other highly-active MoS_2 electrocatalysts in table 1.

The thermodynamics involved in the hydrogen evolution process for MoS_2 have previously been detailed extensively via density functional theory [11]. The active sites for hydrogen evolution in MoS_2 are the sulfur edges. At more positive potentials (>-80 mV versus RHE), proton coverage (number of protons bound to sulfur edges sites) is low and proton adsorption is thermodynamically downhill, but proton reduction is thermodynamically unfavorable due to the strength of S–H bonds. At more negative potentials (<-80 mV versus RHE), proton coverage is higher, so both proton adsorption and proton reduction to yield H_2 are thermodynamically favorable. The -100 mV versus RHE onset of hydrogen evolution for IPL-MoS_2 is consistent with these calculations and suggests that IPL-MoS_2 effectively minimizes energetic and kinetic barriers for HER in contrast with bulk crystalline MoS_2 for which hydrogen evolution begins around -200 mV versus RHE.

HER kinetics can be expressed by the following three steps: the Volmer step (adsorption of proton onto the catalyst surface), the Heyrovsky step (combination of an adsorbed hydrogen with an electron and solution proton), or alternatively the Tafel step (combination of two adsorbed hydrogens). Combination of either the Volmer and Heyrovsky steps or the Volmer and Tafel steps yields H_2. Tafel slopes are used to give insights into the rate-limiting step for a given HER catalyst. However, determination of the HER mechanism from the Tafel slope alone is unfeasible as multiple mechanisms often occur simultaneously. Nevertheless, the significant difference between the Tafel slopes of IPL-MoS_2 and bulk crystalline MoS_2 (figure 5(B)) implies vastly different surface chemistry between the two materials with IPL-MoS_2 having faster reaction kinetics. The Tafel slope observed for IPL-MoS_2 is in line with Tafel slopes previously reported for other highly-active MoS_2 catalysts (~60 mV dec^{-1}) [34, 36, 39]. On other hand, the Tafel slope for bulk MoS_2 is around 90.6 mV dec^{-1}. These results indicate that the proton adsorption is the limiting step for the bulk MoS_2.

Included for comparison purposes in figure 5 are the polarization curves and Tafel plots for platinum metal (Pt) and bare GCE substrate. Platinum, which is currently regarded as the best HER catalyst, significantly outperforms both IPL-MoS_2 and bulk crystalline MoS_2 in terms of onset,

overpotential, and Tafel slope. Although the performance gap between IPL-MoS_2 and Pt remains significant, IPL-MoS_2 represents significant progress when compared to bulk crystalline MoS_2.

In order to investigate the long-term durability of the IPL-MoS_2 material under reductive operating conditions, the material was cycled from 0.1 to −0.35 and back to 0.1 V versus RHE 1000 times. Throughout this extended cycling, an LSV was taken periodically in order to quantify the performance/degradation of the material at various points. Figure 6 compares polarization curves taken immediately after activation and after 1000 reductive cycles. The overpotential of the material increases by only 28 mV after 1000 cycles, implying high stability for HER in acidic media.

4. Conclusions

In conclusion, we report an extremely rapid and benign way to prepare a class of MoS_2 catalysts using an IPL technique. The precursor can be readily converted to MoS_2 with short pulses of light in a few seconds. The conversion of the precursor was demonstrated with XRD and Raman. TEM analysis confirmed that the IPL processed MoS_2 had multiple edge sites that would be beneficial to the HER reaction. A large amount of defect states presented by varying sulfur species at the defects was shown with XPS and confirms the mechanism of improved HER. This presents a significant opportunity to prepare several classes of catalysts that are practically feasible and do not employ vacuum or hydrothermal techniques.

Acknowledgments

This material is based upon work supported by the National Science Foundation under Grant No. 1800245. The authors acknowledge the Conn Center for Renewable Energy Research at the University of Louisville for their financial support and research facilities.

ORCID iDs

Thad Druffel https://orcid.org/0000-0002-1412-3023

References

[1] Liang S *et al* 2015 Au and Pt Co-loaded g-C_3N_4 nanosheets for enhanced photocatalytic hydrogen production under visible light irradiation *Appl. Surf. Sci.* **358** 304–12
[2] Crabtree G W, Dresselhaus M S and Buchanan M V 2004 The hydrogen economy *Phys. Today* **57** 39–44
[3] Xia Y *et al* 2017 Engineering a highly dispersed co-catalyst on a few-layered catalyst for efficient photocatalytic H_2 evolution: a case study of Ni $(OH)_2/HNb_3O_8$ nanocomposites *Catal. Sci. Technol.* **7** 5662–9
[4] Wang M *et al* 2018 An amorphous CoS_x modified $Mn_{0.5}Cd_{0.5}S$ solid solution with enhanced visible-light photocatalytic H_2-production activity *Catal. Sci. Technol.* **8** 4122–8
[5] Liang S *et al* 2016 Constructing a MoS_2 QDs/CdS core/shell flowerlike nanosphere hierarchical heterostructure for the enhanced stability and photocatalytic activity *Molecules* **21** 213
[6] Zou X and Zhang Y 2015 Noble metal-free hydrogen evolution catalysts for water splitting *Chem. Soc. Rev.* **44** 5148–80
[7] Merki D *et al* 2011 Amorphous molybdenum sulfide films as catalysts for electrochemical hydrogen production in water *Chem. Sci.* **2** 1262–7
[8] Xiong J *et al* 2015 An efficient cocatalyst of defect-decorated MoS_2 ultrathin nanoplates for the promotion of photocatalytic hydrogen evolution over CdS nanocrystal *J. Mater. Chem.* **3** 12631–5
[9] Bromley R, Murray R and Yoffe A 1972 The band structures of some transition metal dichalcogenides: III. Group VIA: trigonal prism materials *J. Phys. C: Solid State Phys.* **5** 759
[10] Verble J, Wietling T and Reed P 1972 Rigid-layer lattice vibrations and van der waals bonding in hexagonal MoS_2 *Solid State Commun.* **11** 941–4
[11] Hinnemann B *et al* 2005 Biomimetic hydrogen evolution: MoS_2 nanoparticles as catalyst for hydrogen evolution *J. Am. Chem. Soc.* **127** 5308–9
[12] Gopalakrishnan D, Damien D and Shaijumon M M 2014 MoS_2 quantum dot-interspersed exfoliated MoS_2 nanosheets *ACS Nano* **8** 5297–303
[13] Lukowski M A *et al* 2013 Enhanced hydrogen evolution catalysis from chemically exfoliated metallic MoS_2 nanosheets *J. Am. Chem. Soc.* **135** 10274–7
[14] Eda G *et al* 2011 Photoluminescence from chemically exfoliated MoS_2 *Nano Lett.* **11** 5111–6
[15] Devers E *et al* 2002 Hydrothermal syntheses and catalytic properties of dispersed molybdenum sulfides *Catal. Lett.* **82** 13–7
[16] Cummins D R *et al* 2015 Catalytic activity in lithium-treated core–shell MoO_x/MoS_2 nanowires *J. Phys. Chem.* C **119** 22908–14
[17] Bilgin I *et al* 2015 Chemical vapor deposition synthesized atomically thin molybdenum disulfide with optoelectronic-grade crystalline quality *ACS Nano* **9** 8822–32
[18] Kappera R *et al* 2014 Metallic 1T phase source/drain electrodes for field effect transistors from chemical vapor deposited MoS_2 *APL Mater.* **2** 092516
[19] Ponomarev E *et al* 1996 Electrochemical deposition of MoS_2 thin films by reduction of tetrathiomolybdate *Thin Solid Films* **280** 86–9
[20] Li Q *et al* 2004 Polycrystalline molybdenum disulfide (2H–MoS_2) nano-and microribbons by electrochemical/chemical synthesis *Nano Lett.* **4** 277–81
[21] Liu K-K *et al* 2012 Growth of large-area and highly crystalline MoS_2 thin layers on insulating substrates *Nano Lett.* **12** 1538–44
[22] Druffel T *et al* 2018 Intense pulsed light processing for photovoltaic manufacturing *Sol. Energy Mater. Sol. Cells* **174** 359–69
[23] Dharmadasa R *et al* 2013 Room temperature synthesis of a copper ink for the intense pulsed light sintering of conductive copper films *ACS Appl. Mater. Interfaces* **5** 13227–34
[24] Dharmadasa R *et al* 2014 Intense pulsed light treatment of cadmium telluride nanoparticle-based thin films *ACS Appl. Mater. Interfaces* **6** 5034–40
[25] Lavery B W *et al* 2016 Intense pulsed light sintering of $CH_3NH_3PbI_3$ solar cells *ACS Appl. Mater. Interfaces* **8** 8419–26
[26] Li H *et al* 2012 From bulk to monolayer MoS_2: evolution of Raman scattering *Adv. Funct. Mater.* **22** 1385–90
[27] Frey G L *et al* 1999 Raman and resonance Raman investigation of MoS_2 nanoparticles *Phys. Rev.* B **60** 2883

[28] Bozheyev F, Valiev D and Nemkayeva R 2017 Pulsed cathodoluminescence and Raman spectra of MoS_2 nanocrystals at different excitation electron energy densities and laser wavelengths *J. Lumin.* **188** 529–32
[29] Weber T, Muijsers J and Niemantsverdriet J 1995 Structure of amorphous MoS_3 *J. Phys. Chem.* **99** 9194–200
[30] Muijsers J *et al* 1995 Sulfidation study of molybdenum oxide using $MoO_3/SiO_2/Si$ (100) model catalysts and Mo-IV3-sulfur cluster compounds *J. Catal.* **157** 698–705
[31] Wang H *et al* 1997 Synthesis and characterization of molybdenum disulphide formed from ammonium tetrathiomolybdate *J. Mater. Sci.* **32** 497–502
[32] Druffel T *et al* 2018 Intense pulsed light processing for photovoltaic manufacturing *Sol. Energy Mater. Sol. Cells* **174** 359–69
[33] Ankireddy K *et al* 2018 Rapid thermal annealing of $CH_3NH_3PbI_3$ perovskite thin films by intense pulsed light with aid of diiodomethane additive *J. Mater. Chem* A **6** 9378–83
[34] Chen Z *et al* 2011 Core–shell MoO_3–MoS_2 nanowires for hydrogen evolution: a functional design for electrocatalytic materials *Nano Lett.* **11** 4168–75
[35] Wu Z *et al* 2013 MoS_2 nanosheets: a designed structure with high active site density for the hydrogen evolution reaction *ACS Catalysis* **3** 2101–7
[36] Benck J D *et al* 2012 Amorphous molybdenum sulfide catalysts for electrochemical hydrogen production: insights into the origin of their catalytic activity *ACS Catal.* **2** 1916–23
[37] Xie J *et al* 2013 Defect-rich MoS_2 ultrathin nanosheets with additional active edge sites for enhanced electrocatalytic hydrogen evolution *Adv. Mater.* **25** 5807–13
[38] Li Y *et al* 2011 MoS_2 nanoparticles grown on graphene: an advanced catalyst for the hydrogen evolution reaction *J. Am. Chem. Soc.* **133** 7296–9
[39] Jaramillo T F *et al* 2007 Identification of active edge sites for electrochemical H_2 evolution from MoS_2 nanocatalysts *Science* **317** 100–2